ACS APPLIED MATERIALS & INTERFACES

Research Article

www.acsami.org

Shape-Controlled Synthesis of Silver Nanocrystals by X-ray Irradiation for Inkjet Printing

Hsien-Tse Tung,[†] In-Gann Chen,[‡] Ivan M Kempson,[†] Jenn-Ming Song,[§] Yu-Feng Liu,[‡] Po-Wei Chen,[‡] Weng-Sing Hwang,[‡] and Yeukuang Hwu*,[†]

[†]Institute of Physics, Academia Sinica, Taipei, Taiwan

[‡]Department of Materials Science and Engineering, National Cheng Kung University, Tainan, Taiwan

[§]Department of Materials Science and Engineering, National Chung Hsing University, Taichung, Taiwan

Supporting Information

ABSTRACT: A suite of silver (Ag) nanocrystals have been synthesized using a rapid water radiolysis approach via X-ray irradiation. Various shapes including spheroidal, prism, rod, and multifaceted nanoparticles can be produced by varying the initial concentration of polyvinylpyrrolidone (PVP) relative to silver nitrate ($AgNO_3$). UV−visible spectroscopy and transmission electron microscopy (TEM) coupled with selected area electron diffraction (SAED) have been used to characterize these Ag products. At an optimized reagent ratio, a mixture of high-aspect-ratio rods (tunable to ∼50) and spheroidal particles result. Such a mixture is proven to have highly beneficial melting point and dispersive properties suited to inkjet printing of conductive Ag lines. The resistivity of the printed lines decreases to 77.7 $\mu\Omega$ and 33.1 $\mu\Omega$ after heating to 200 and 350 °C.

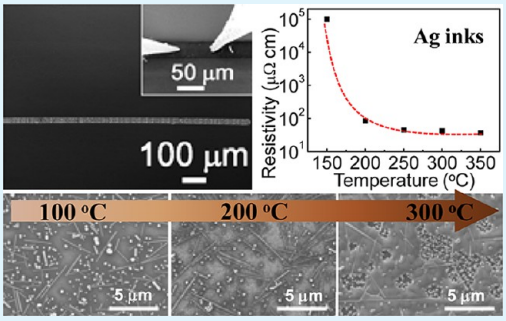

KEYWORDS: *silver nanocrystals, silver nanowires, shape control, X-ray irradiation, inkjet printing*

1. INTRODUCTION

Controlling size and morphology of nanostructures is of both fundamental and technological interest for providing effective strategies to tune electronic and optical properties of materials.[1−4] Nanostructures made of noble metal, such as Ag,[5,6] gold,[7−9] and platinum,[10,11] are of particular interest because of their unique respective properties. Ag possesses the highest electrical and thermal conductivity among all the metals. Along with other properties, these promote extensive use in catalysis,[12,13] electronics,[14,15] photonics,[16] photography,[17] biological labeling,[18,19] optical sensing,[20,21] and antimicrobials.[22]

Recently, using Ag nanoparticles to produce conductive tracks with inkjet printing has attracted attention due to its high conductivity and thermal stability.[23−25] Direct writing or drop-on demand technology represents a new method in which nanoparticles are directly printed on a substrate using inkjet printing technology. A post-heating step is used to sinter or melt the nanoparticles to impart continuity and conductivity to the track. Methods for producing high quality, continuous tracks which reflect the conductivity of bulk Ag and are formed at low temperatures attracts abundant interest. Challenges arise in achieving uniform deposition and continuity in conductivity and lowering heat treatment temperatures to broaden the range of viable substrates. With evaporation of the solvent from a drop of dilute nanoparticle solution, the solid particles have an energetic preference to accumulate at the droplet edge; assembling into a ring or discontinuous track.[26] Subsequently, a combination of small spheroidal and anisotropic Ag nanocrystals are shown here to overcome this complication and promote continuous conductive tracks with low melting points. Demonstrated use of comixtures in inkjet printing is currently limited. However, we present through the method described here, chemical reactants can be used to tune synthesis conditions to produce mixtures of both types of nanoparticles simultaneously, rapidly and of size scale to promote low temperature sintering. This dramatically simplifies production of high-performance colloidal solutions that can be directly applied to a variety of substrates for printing conductive tracks.

In the common synthesis of Ag nanocrystals by the polyol method, PVP has proven to be convenient and often favorable. Some important PVP-assisted methods for the synthesis of shape-controlled Ag nanocrystals and their operating parameters are summarized in Table S1 in the Supporting Information.[27−32] These Ag nanoscale disks,[27] prisms,[28] cubes,[29] and wires[30−32] are mainly synthesized with input of heat energy. Our method utilizes irradiation with X-rays, which generates a redox environment due to radicalization of solvent molecules,[33] in this case, water. Upon X-ray irradiation, water dissociates to form highly reactive radicals and can be used for reduction of metal ions to form nanoparticles.[34−38] This has alternatively been performed with ultrasonic reduction[39] and γ-

Received: August 6, 2012
Accepted: October 16, 2012
Published: October 16, 2012

ray irradiation.[40] The resulting hydrogen radicals ($H^{\bullet}$) and solvated electrons (e^{-}_{aq}) are powerful reducing agents and rapidly reduce Ag^{+} ions to Ag atoms. This approach offers several advantages including low temperature and rapid synthesis, uniform reaction kinetics, and no need for addition of a chemical reducing agent (subsequently improving nanoparticle purity). These benefits provide flexibility and control in synthesis and complete synthesis requires only a few minutes. We show here that anisotropy assists in uniform deposition of Ag into homogeneous tracks. The size and dimensions of the nanoparticles further promote conductivity by enabling low-temperature melting.

In this work, PVP-coated and stabilized Ag seeds <10 nm in diameter were formed in solution as nucleation sites by irradiation for 5 s (see Figure S1 in the Supporting Information). Subsequent growth was performed with attenuation of the X-ray beam with a 1.6 mm thick aluminum plate for 10 min. Adjusting the relative concentration of PVP enabled the synthesis of various colloidal structures (spherical, prism, or rod/wire nanoparticles). Formation of an appropriate seed can be used to form particle and wire mixtures.

2. EXPERIMENTAL SECTION

Silver nitrate ($AgNO_3$, 99+%), polyvinylpyrrolidone (PVP, 99.5%, molecular weight ~40 000 g/mol), and methanol (99.8%) were purchased from Aldrich (MO, USA). All chemicals were used without further purification. Polished silicon (100) wafers were obtained from Silicon Sense (NH, USA). Precleaned glass slides were purchased from Corning Glass (NY, USA).

Ag nanostructures were synthesized in solution as follows. A 4 mL solution containing 9 mM silver nitrate ($AgNO_3$), poly vinylpyrrolidone (PVP) of various concentrations (9 mM, 18 mM, 36 mM and 45 mM) and water was mixed in a glass vial. PVP (monomeric unit ~111 g/mol) was added to provide PVP/$AgNO_3$ molar ratios of 1, 2, 4, and 5. The whole reaction including nucleation and growth stages were conducted in the same vial with no further addition of reagents.

For nucleation, the aforementioned mixture was irradiated by intense X-rays for 5 s at the 'white light' BL01A beamline of the National Synchrotron Radiation Research Center, Hsinchu, Taiwan, with an electron storage ring current of 360 mA. The photon energy distribution was centered at 10−15 keV and the dose rate was 5.1 ± 0.9 kGy s^{-1} as determined by a Fricke dosimeter with an estimated G-value of 13.[38] The irradiated solution with Ag seeds showed a light yellow color.

Subsequent growth was conducted by immediately placing 1.6 mm thick aluminum sheet in front of the solution to attenuate the X-ray beam. The attenuation varies radical concentrations and reaction rates. In this case, high X-ray flux was found to be counterproductive for the subsequent nanocrystal growth stage. During the crystal growth, the solution was irradiated for up to 20 min at room temperature without stirring.

After irradiation, the solution was centrifuged at 6000 rpm for 10 min and washed with methanol and resuspended 3 times to remove residual PVP. The synthetic yield was ~1.5 wt %. The precipitate of Ag nanostructures was collected and redispersed to form concentrated (15 wt %) Ag inks. The inks were printed by an inkjet printer on silicon and glass substrates. The substrates were cleaned with acetone and deionized water to remove particulates and organic contaminates from the surface. After cleaning, the substrates were treated with UV/O_3 for 30 min for better surface contact (Figure S2 in the Supporting Information). After printing, the patterned structures were heated at different temperatures, from 100 to 350 °C with an interval of 50 °C for 1 h.

The printer setup consisted of a drop-on demand piezoelectric inkjet nozzle. A squeeze mode piezoelectric print head MJ-AT-01 manufactured by MicroFab Technologies Inc., was employed in this study. The diameter of the print head nozzle orifice is 20 μm and was operated with a typical bipolar pulse waveform which can minimize unwanted satellite droplets and asymmetric droplet formation. The waveform was set to 2, 5, 2, 5, and 2 μs for rise, dwell, fall, echo and final times as illustrated in the diagram in Figure S3 of the Supporting Information. A slow rising time is used to prevent air from being sucked into the tube and sufficient interval time between droplet formations was designed for meniscus oscillations to dissipate completely. The driving voltage was set as ±20 V, and the single droplet volume is ~2×10^{-14} m^3. During the printing process, the gap between print head and substrate on the planar moving stage was adjusted to 5 mm, and the patterns were printed on a computer-controlled gantry system capable of movement accurate to ±5 μm. The straight lines were constructed with the dot spacing of 40 and 60 μm (Figure S4 of SI). All patterns were printed with the stage velocity of 10 mm/s. The viscosity and surface tension of the concentrated Ag ink were measured by a viscometer (model DV-II+Pro, Brookfield) and tensiometer (K10ST, Krüss Gmbh). The viscosity and surface tension of the three types of Ag inks in this study were ~1.4 mPa s and ~37.1 mN m^{-1}. A squeeze-mode piezoelectric printhead MJ-AT-01 is manufactured by MicroFab Technologies Inc.

The structure and diffraction pattern of the nanostructures were characterized respectively using a transmission electron microscope (TEM, JEM-2100F) with an accelerating voltage of 200 kV. The morphology and size distribution were obtained using a scanning electron microscope (SEM, Zeiss EVO50) with an accelerating voltage of 20 kV. An atomic force microscope (AFM, Seiko SPA300HV) with a 1 Hz scan rate was used to examine the roughness of the patterned structures. The melting points of the silver solutions were analyzed by differential scanning calorimetry (DSC) at a heating rate of 10 °C/min under ambient atmosphere. Before DSC experiments, all the samples were heated at 100 °C for 1 h to evaporate methanol and subsequently cooled to the ambient temperature. The current−voltage measurements of the patterns were controlled by two nanomanipulators (Klocke Nanotechnik) with tungsten tips and carried out using a Keithley 236 source measurement unit.

3. RESULTS AND DISCUSSION

Figure 1a shows the evolution of UV−visible absorption spectra with synthesis time taken from a solution containing a molar ratio of PVP/$AgNO_3$ of 2. Corresponding TEM images are given in Figure 1b-d. With X-ray irradiation for 1 min, the UV−visible spectrum is dominated by a peak at ~410 nm indicating formation of a Ag colloid.[32] With further irradiation from 5 to 10 min, distinct anisotropy occurs. The TEM image after 5 min irradiation (Figure 1b) identifies multifaceted nanoparticles (termed multiply twinned particles[32]) with 5-fold symmetry (see Figure S5 in the Supporting Information) and Ag nanorods. The degree of anisotropy can be adjusted with irradiation time. As shown after 10 min (Figure 1c), the products can develop dramatically higher aspect ratio (~50 with dimensions of 5 μm × 100 nm). Simultaneously, other spheroidal Ag crystals approach a homogeneous size without forming the wire-shaped crystals. Structural analysis of the Ag nanowires was performed by selected area electron diffraction (SAED) and high resolution TEM (HRTEM) analyses. Images d and e in Figure 1 show a high-magnification TEM image of an Ag nanowire and its SAED pattern, respectively. The SAED pattern confirms that nanowire growth occurs along the $[1\bar{1}0]$ direction. Most of the spots can be indexed to one of the two zone axes of the Ag structure, the [110] zone axis (indexed using bold characters) and [111] zone axis (italic characters). These indicate that the nanowire is not a single domain crystal but has a twinned structure, similar to that reported previously and highlighted in Figure 1f.[30−32] A clear twin boundary can be seen, showing the existence of a twin plane inside the wire.

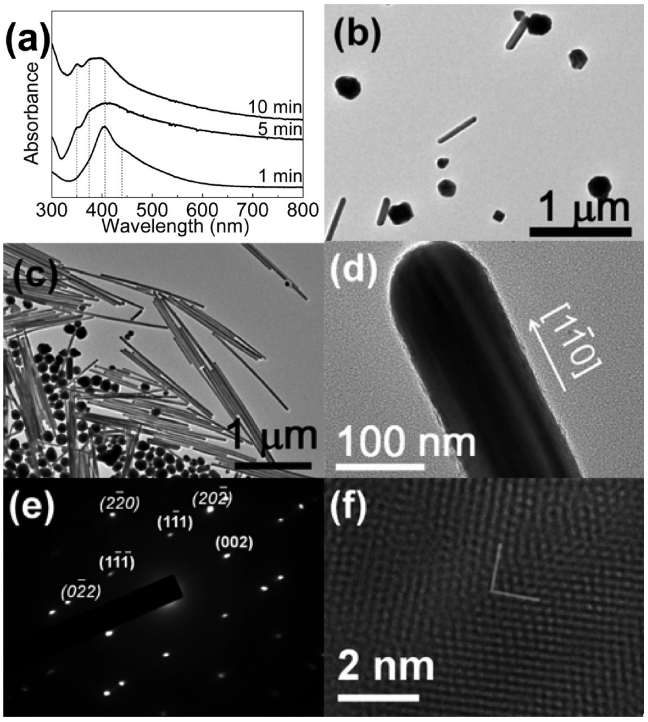

Figure 1. Ag nanostructures formed with a PVP/$AgNO_3$ molar ratio of 2. (a) UV−visible absorption spectra after synthesis for 1, 5, and 10 min. Corresponding products are shown by TEM after (b) 5 and (c) 10 min. (d) High-magnification TEM image of the Ag nanowire and (e) its SAED pattern. Most of the diffraction spots can be indexed to one of the two sets: the [110] zone axis (indexed using bold characters) and [111] zone axis (italic characters) of Ag, indicating the nanowire is a twinned structure. (f) HRTEM image taken from the Ag nanowire confirms a twinned structure.

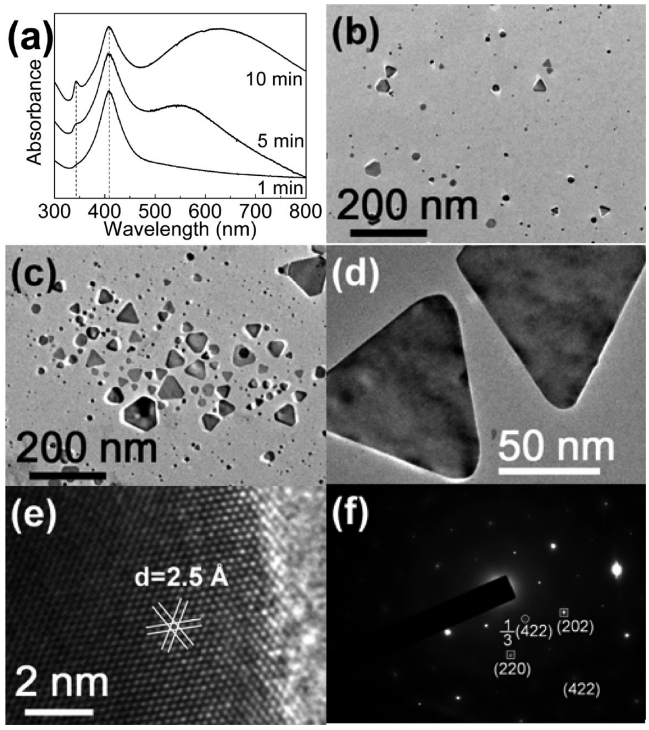

Figure 2. Ag nanostructures formed with a PVP/$AgNO_3$ molar ratio of 4. (a) UV−visible absorption spectra after synthesis for 1, 5, and 10 min. Corresponding products are shown by TEM after (b) 5 and (c) 10 min. (d) High-magnification TEM image of Ag nanoprisms and (e) a HRTEM image of an edge with (f) corresponding SAED pattern. The strong spots (square) could be indexed to the allowed {220} reflection, and the inner spots (circle) with a weak intensity corresponding to the formally forbidden (1/3){422} reflection.

By increasing the molar ratio of PVP/$AgNO_3$ to 4, triangular nanoprisms become the major product (Figure 2). Figure 2a shows the UV−visible absorption spectra of the nanoprisms. After the first minute of irradiation, one significant peak centered at 410 nm is present, corresponding to the dipole resonance of Ag nanoparticles, whereas the out-of-plane (340 nm) quadrupole resonance is unapparent.[28] With irradiation for 5 and 10 min, the out-of-plane quadrupolar plasmon-resonance band at 340 nm gradually appears and the sensitive in-plane dipole plasmon-resonance undergoes a bathochromic shift from ~555 nm to ~645 nm. This corresponds with the edge length of the prisms growing from 37 ± 4 nm to 87 ± 9 nm (Figure 2b and 2c). The broadened dipole in-plane plasmon-resonance band can result from the increase of the size distribution and the differences in shape (truncated or acute) of the nanoprisms.[28] Imaging the near edge of a single prism (Figure 2d) with HRTEM is shown in Figure 2e. A corresponding SAED pattern obtained from a single Ag nanoprism lying flat on the support film with the incident electron beam perpendicular to the triangular facets is shown in Figure 2f. The fringes are separated by 2.5 Å, which can be ascribed to the (1/3){422} reflection that is generally forbidden for an fcc lattice. The 6-fold rotational symmetry displayed by the diffraction spots implies that the triangular faces are representing the {111} planes.

Other molar ratios of PVP/$AgNO_3$ were also investigated. Multifaceted or spherical nanoparticles were obtained for ratios above or below those described above. Figure 3a shows UV−visible absorption spectra of Ag nanoparticles produced with a PVP/$AgNO_3$ ratio of 1. The absorption peak broadened and shifted to 456 nm after 10 min. The corresponding images (Figure 3b, c) to the 5 and 10 min curves in Figure 3a indicate the formation of different shapes of nanocrystals with a very broad size distribution.[41] For a ratio of 5 (Figure 3d−f), the absorption peak grew and gradually shifted to 415 nm, suggesting continuous population growth of Ag nanoparticles with reasonably uniform size. Images e and f in Figure 3 show TEM images of the Ag nanoparticles corresponding to the 5 and 10 min curves in Figure 3d, respectively. The images show a homogenization of the nanoparticles toward a narrower size distribution.

Generally, fast reduction of the metal ions (e.g., reaction with powerful reducing agents such as radicals) results in spherical colloids in which the surfaces of the nanoparticles typically exhibit a mixture of {111} and {100} planes.[42] To minimize their overall energy, the seeds undergo twinning, in which stacking faults are formed within the crystal matrix. In the present study, we propose that the degree of seed crystal twinning is critical to the final morphology of the nanostructures and is reliant on the relative PVP concentration. With the molar ratio of PVP/$AgNO_3$ at 2, multifaceted Ag seeds with a decahedral shape were found at the nucleation stage. Once the multifaceted seeds have formed, reduced Ag atoms will continuously deposit on the surface of the {111} facet, and subsequently form a new {110} facet. Because of Ostwald ripening, the nanoparticles will grow continuously to form a one-dimensional nanostructure.[32] In contrast, with

dx.doi.org/10.1021/am3015718 | ACS Appl. Mater. Interfaces 2012, 4, 5930−5935

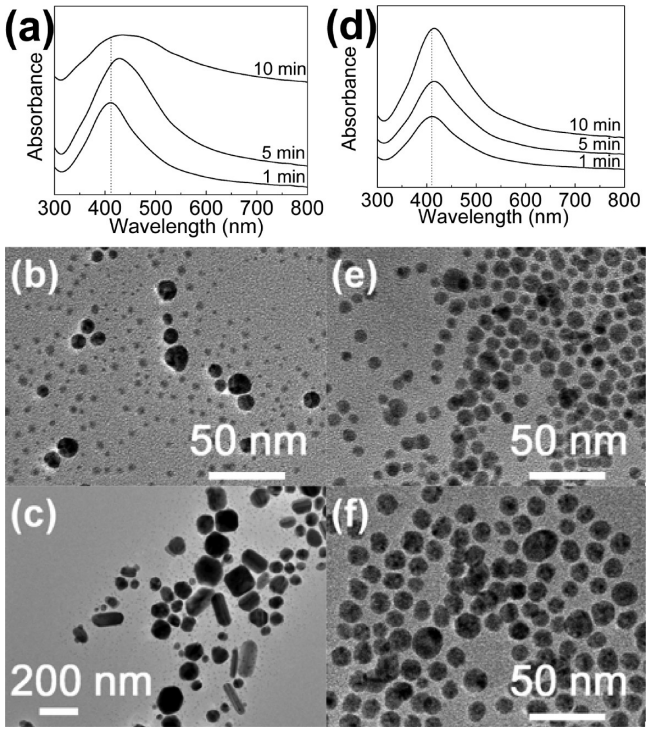

Figure 3. Ag nanostructures formed with a PVP/$AgNO_3$ molar ratio of (a–c) 1 and (d–f) 5. (a, d) UV–visible absorption spectra after synthesis for 1, 5, and 10 min. Corresponding TEM images of the Ag nanostructures obtained by irradiating the solution for (b, e) 5 and (c, f) 10 min.

increasing the molar ratio of PVP/$AgNO_3$ to 4, triangular nanoprisms appear in solution instead. From previous reports, it was believed that nanoprism crystal growth can only occur when the initial seeds contain one or two twin planes parallel to the major {111} facets.[43] This atomic arrangement initially results in {111} faceted reentrant grooves on the sides of the crystal plates, providing nucleation sites for deposition of new crystal layers and drives plate-like crystal growth.[44] We therefore conclude that the seed structure is governing the shape and crystal structure of the final nanostructures. However, how the PVP concentration affects the degree of crystal twinning is still under investigation. One possible function of PVP is to influence the growth rates of the seeds. PVP could also alter radical concentrations under irradiation and affect the synthesis, or act to terminate preferential crystal faces. If PVP contributes to the reaction, then a concentration related effect could be expected. For example, at a relatively low PVP concentration the nucleation of Ag seeds is such that 5-fold symmetric multifaceted particle growth is promoted; on the other hand, a relatively high PVP concentration only allows one or two twin planes because of the difference in nucleation dynamics and kinetics.

Moreover, regardless of the molar ratio of PVP to $AgNO_3$ lower than 2 or higher than 4, no nanowires or nanoprisms are formed even after prolonged irradiation for 20 min. With the molar ratio of PVP to $AgNO_3$ lower than 2, the PVP concentration is presumably too low for the surface area of the nanoparticles and cannot interact sufficiently with all of the Ag crystal facets. In the end, the Ag crystals develop in different shapes with uncontrollable particle shape and size distribution. When the molar ratio of PVP/$AgNO_3$ is higher than 4, high coverage of PVP appears to limit the growth rate on all planes of the Ag nanocrystals, leading to the gradual isotropic growth mode and finally, spherical products.[32] In the intermediate scenario, a bicomponent seed mixture results in simultaneous wire and spheroidal particle formation. Note that the aforementioned 410 nm peak in the UV–visible spectra (similar to Patakfalvi et al.[45]) is present in all samples regardless of their PVP/$AgNO_3$ precursor molar ratios and the X-ray irradiation exposure. This result indicates that abundant small Ag nanoparticles exist in the solution with other wire or prism type particles. This morphology of mixed particles of different size and shape is also confirmed with high magnification TEM images (see Figure S6 in the Supporting Information).

Although various functionalities based on size and shape may entail from these colloids, the mixture of wires and spherical nanoparticles were explored for beneficial physical properties for printing conductive Ag lines. The inclusion of wires was expected to promote the formation of continuous, conductive tracks. Lines of nanoparticles were printed on silicon wafer by inkjet printing to compare the three different kinds of "inks" (i.e., the nanowire mixture, nanoprisms, and spheroidal colloid solutions) to assess dependence on morphologies in assisting conductivity.

Figure 4a shows a representative SEM image of a printed line of nanoparticles after heating to 250 °C having a width of ~29.7 μm and height of 150 nm measured by atomic force microscopy (AFM). With 40 μm of interspacing distance between dots on the silicon wafer, the line is well connected (see Figure S4 in the Supporting Information). The AFM measurement in Figure 4b confirms a smooth surface profile thick in the middle and thin on the edges. The line width also decreases with heating which could be attributed to the rapid evaporation in the heating process. Current–voltage (I–V) curves of the printed lines were measured for various distances between two tungsten tips placed along the wire direction (inset of Figure 4a). From this, the resistance (R) corresponding to a given length (L) can be measured. The corresponding I–V curve of Figure 4a is shown in Figure S7 in the Supporting Information. Upon removal of the distance-dependent resistance, the intrinsic resistivity (ρ) of the nanowire mixture line was calculated as 41.3 $\mu\Omega$ cm (based on an integrated cross-sectional area of A = 4.1 μm^2, inset of Figure 4b, and the value $\Delta R/\Delta L$ = 755.1Ω/75 μm, according to the equation $\rho = \Delta R \times A/\Delta L$). Figure 4c compares resistivity as a function of heating temperature. Significant reduction in resistivity to 77.7 $\mu\Omega$ cm occurred with heating at 200 °C and reached a minimum value of 33.1 $\mu\Omega$ cm after reaching ~350 °C (compared to that of the pure bulk Ag: 1.6 $\mu\Omega$ cm).

The Ag mixture of wires and spherical nanoparticles were analyzed using DSC in a temperature range of 30 to 350 °C (Figure 4d). Two endothermic peaks at about 170 and 270 °C could be attributed with different phase changes of different-sized Ag nanoparticles with the PVP on the surfaces. Although the decomposition temperature of PVP (>400 °C) and the melting temperature of Ag (>900 °C) are all much higher than this temperature range, we cannot rule out that the interface modification in the PVP-Ag nanoparticle complex could induce thermal properties different from that of the individual components. For gold nanoparticles of 10 nm diameter, features in a similar temperature range have been proposed to arise from pyrolysis of the stabilizing PVA polymer.[46] We also note that very small Ag nanoparticles (<2 nm) were present in each solution (see Figure S6 in the Supporting

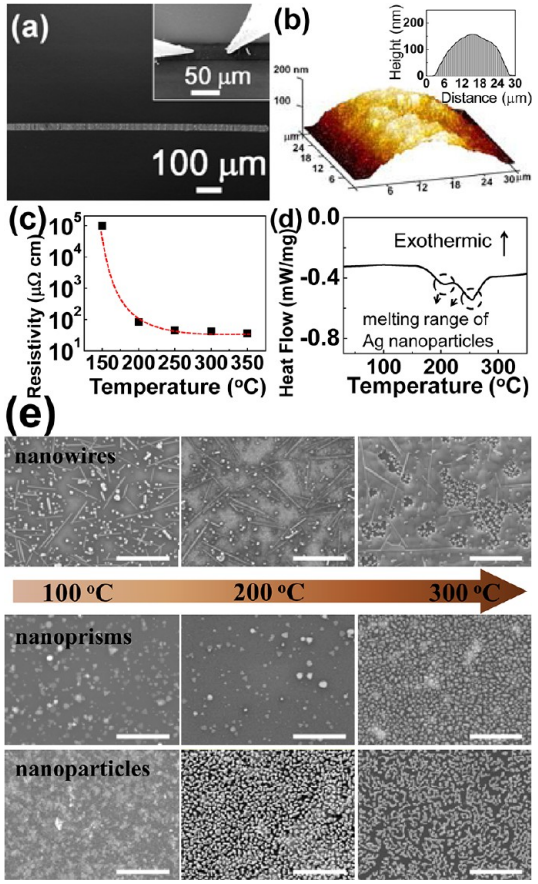

Figure 4. Printing conductive tracks. (a) SEM image of a printed line in contact with two tungsten electrodes (inset), and (b) corresponding AFM determination of topography. (c) The resistivity decreases as a function of heating temperature for sol containing nanowires. (d) The DSC curve upon heating of the Ag nanowire dominated products used in this study. (e) SEM images showing the microstructure of Ag nanowire dominated products (top), nanoprisms (middle), and nanoparticles (bottom) heated at 100, 200, and 300 °C for 1 h. All scale bars = 5 μm.

Information) and that could contribute to the low temperature features in DSC data as some references suggested.[47−49] Data from DSC can give indications of many processes including melting, sintering, phase transitions and degradation, thus interpretation of the DSC curve is confounded by many factors. Theoretical models predict that metal nanoparticle melting points can be significantly altered and confounded by many factors including shape[50] and substrate material (contact angle)[51] and increase in uncertainty with decreasing nanoparticle size. Kim et al., have experimentally shown silver nanoparticle melting points range from 112 to 193 °C for the size range of 3.5−6.6 nm diameter.[52] In our case, the SEM images given in Figure 4e and Figure S8a of the Supporting Information clearly show that fusion of the nanoparticles occurs below 300 °C. It is tempting to associate the two features in the DSC curve to melting of two different size distributions of nanoparticles. However, we remain unable to conclusively discern the exact contributions to this curve and there may be contribution from the stabilizing polymer such as a glass transition.[53] Collectively, these observations indicate complexity for small nanoparticles exhibiting intricacies in physical properties that provide challenges theoretically and instrumentally to elucidate specific processes. These points raise questions worthy of further investigation in regards to modeling, polymer, and metal nanoparticle behavior in this size and temperature regime.

Because the PVP capping is too stable to decompose below 350 °C, it is unlikely to exhibit purely sintering behavior. SEM images reveal that the nanowire colloids produce conductive tracks compared to the other samples (Figure 4e).

The importance of the particle and wire mix is particularly evident when comparing printed lines as a function of temperature with SEM (Figure 4e). Although the Ag nanoparticles start melting slightly above 160 °C for each morphology, the formation of long-range conductive tracks does not occur without incorporating wires. Instead, the Ag nanoprisms and nanoparticles in the patterned line are likely to be isolated dots. High magnification SEM images of these three kinds of Ag solution heated at 300 °C clearly show that with the inclusion of Ag nanowires, the fused nanoparticles are bridged by the nanowires. On the other hand, at the same temperature, Ag nanoprisms and nanoparticles solution form short-range conductive tracks but highly discontinuous (see Figure S8 in the Supporting Information). The corresponding $I-V$ curve of these lines further show a Schottky barrier effect of tungsten−silicon-tungsten contact (see Figure S9 in the Supporting Information), which suggests electron flow is via a silicon path rather than Ag.

We have also tested printing inks on a glass substrate to compare data from a more economical substrate. The printed lines are of lower quality (see Figure S10 in the Supporting Information) than on silicon surface and this result indicates the importance of optimizing condition between ink and substrates as well as the alignment of the inkjet printer. The annealing temperature of 200 °C can enable printing on some polymer surfaces. However, for versatility and provision of using a broader range of polymer substrates this temperature still needs to be further reduced. We have found that adding $AgNO_3$ to Ag nanowire mixture solutions can produce denser Ag patterns and better conductive performance after heating at 200 °C. Further optimization is underway.

4. CONCLUSION

In summary, we have developed an X-ray irradiation technique to rapidly synthesize Ag nanostructures at room temperature. It was found that the molar ratio between $AgNO_3$ and PVP plays a critical role in the structure of seeds which consequently relate to formation of different products (nanowires mixture, nanoprisms, or spherical nanoparticles). Inkjet printing of Ag nanowire mixture solutions exhibited low resistivity, ranging from 77.7 $\mu\Omega$ cm to 33.1 $\mu\Omega$ cm when heated at 200−350 °C. Existence of Ag nanowires in the colloidal solution was critical for fusing particles to form long-range conductive tracks.

■ ASSOCIATED CONTENT

Ⓢ Supporting Information

Additional images and the $I-V$ curves of printed line made of Ag nanocrystals. This material is available free of charge via the Internet at http://pubs.acs.org.

■ AUTHOR INFORMATION

Corresponding Author

*Phone: + 886-2-2789-6721. E-mail: phhwu@gate.sinica.edu.tw, phhwu@phys.sinica.edu.tw.

Notes

The authors declare no competing financial interest.

■ ACKNOWLEDGMENTS

This work was supported by the National Science Council of Taiwan (grant NSC 98-2120-M-001-002), by the Academia Sinica (Taiwan), by the Swiss Fonds National and by the Centre d'Imagérie Biomédicale (CIBM). Technical supports from NanoCore, the Core Facilities for Nanoscience and Nanotechnology at Academia Sinica in Taiwan, as well as Center for Energy Technology and Strategy, National Cheng Kung University in Taiwan, are acknowledged. We also thank Dr. Chuan-Ming Tseng for his assistance in TEM analysis.

■ REFERENCES

(1) Frank, S.; Poncharal, P.; Wang, Z. L.; de Heer, W. A. *Science* **1998**, *280*, 1744.
(2) Yu, K.; Ouyang, J.; Zhang, Y.; Tung, H. T.; Lin, S.; Nagelkerke, R. A. L.; Kingston, D.; Wu, X.; Leek, D. M.; Wilkinson, D.; Li, C.; Chen, I. G.; Tao, Y. *ACS Appl. Mater. Interfaces* **2011**, *3*, 1511.
(3) Duan, X.; Huang, Y.; Cui, Y.; Wang, J.; Lieber, C. M. *Nature* **2001**, *409*, 66.
(4) Huang, H. M.; Mao, S.; Feick, H.; Yan, H.; Wu, Y.; Kind, H.; Weber, E.; Russo, R.; Yang, P. *Science* **2001**, *292*, 1897.
(5) Tung, H. T.; Chen, I. G.; Song, J. M.; Yen, C. W. *J. Mater. Chem.* **2009**, *19*, 2386.
(6) Tung, H. T.; Song, J. M.; Feng, S. W.; Kuo, C.; Chen, I. G. *Phys. Chem. Chem. Phys.* **2010**, *12*, 740.
(7) Ji, C.; Searson, P. C. *Appl. Phys. Lett.* **2002**, *81*, 4437.
(8) Olson, T. Y.; Zhang, J. Z. *J. Mater. Sci. Technol.* **2008**, *24*, 433.
(9) Tung, H. T.; Song, J. M.; Nien, Y. T.; Chen, I. G. *Nanotechnology* **2008**, *19*, 455603.
(10) Kuo, P. L.; Hsu, C. H. *ACS Appl. Mater. Interfaces* **2011**, *3*, 115.
(11) La-Torre-Riveros, L.; Guzman-Blas, R.; Méndez-Torres, A. E.; Prelas, M.; Tryk, D. A.; Cabrera, C. R. *ACS Appl. Mater. Interfaces* **2012**, *4*, 1134.
(12) Bastide, S.; Quang, N. L.; Monna, R.; Lévy-Clément, C. *Physica Status Solidi (C)* **2009**, *6*, 1536.
(13) Mathiyarasu, J.; Phani, K. L. N. *J. Electrochem. Soc.* **2007**, *154*, B1100.
(14) Kim, W. T.; Jung, J. H.; Kim, T. W.; Son, D. I. *Appl. Phys. Lett.* **2010**, *96*, 253301.
(15) Zhou, W.; Ren, L.; Lin, F.; Jiao, L.; Xue, T.; Xian, X.; Liu, Z. *Appl. Phys. Lett.* **2008**, *93*, 123115.
(16) Singh, S. P.; Karmakar, B. *Plasmonics* **2011**, *6*, 457.
(17) Espiau de Lamaestre, H.; Béa; Bernas, R. H.; Belloni, J.; Marignier, J. L. *Phys. Rev. B* **2007**, *76*, 205431.
(18) Adam, C.; Garnier-Laplace, J.; Baudin, J. P. *Water, Air, Soil Pollut.* **2002**, *136*, 125.
(19) Lee, S. Y.; Jang, S. H.; Cho, M. H.; Kim, Y. M.; Cho, K. C.; Ryu, P. D.; Gong, M. S.; Joo, S. W. *J. Microbiol. Biotechnol.* **2009**, *19*, 9.
(20) Geng, Z.; Liu, W.; Wang, X.; Yang, F. *Sens. Actuators, A: Phys.* **2011**, *169*, 37.
(21) Mohammad, R. A.; Reza, A. *Sensor Lett.* **2010**, *8*, 777.
(22) Sreelakshmi, C.; Datta, K. K. R.; Yadav, J. S.; Reddy, B. V. S. *J. Nanosci. Nanotechnol.* **2011**, *11*, 6995.
(23) Jeong, S.; Song, H. C.; Lee, W. W.; Choi, Y.; Ryu, B. H. *J. Appl. Phys.* **2010**, *108*, 102805.
(24) Park, S. K.; Kim, Y. H.; Han, J. I. *Org. Electron.* **2009**, *10*, 1102.
(25) Aggarwal, R.; Narayan, R. J.; Xiao, K.; Geohegan, D. B. *J. Vac. Sci. Technol. B* **2008**, *26*, L48.
(26) Layani, M.; Gruchko, M.; Milo, O.; Balberg, I.; Azulay, D.; Magdassi, S. *ACS Nano* **2009**, *3*, 3537.
(27) Tang, B.; An, J.; Zheng, X.; Xu, S.; Li, D.; Zhou, J.; Zhao, B.; Xu, W. *J. Phys. Chem. C* **2008**, *112*, 18361.
(28) Pastoriza-Santos, I.; Liz-Marzán, L. M. *Nano Lett.* **2002**, *2*, 903.
(29) Zhao, T.; Fan, J. B.; Cui, J.; Liu, J. H.; Xu, X. B.; Zhu, M. Q. *Chem. Phys. Lett.* **2011**, *501*, 414.
(30) Sun, Y.; Mayers, B.; Herricks, T.; Xia, Y. *Nano Lett.* **2003**, *3*, 955.
(31) Sun, Y.; Gates, B.; Mayers, B.; Xia, Y. *Nano Lett.* **2002**, *2*, 165.
(32) Sun, Y.; Yin, Y.; Mayers, B.; Herricks, T.; Xia, Y. *Chem. Mater.* **2002**, *14*, 4736.
(33) Tung, H. T.; Hwu, Y.; Chen, I. G.; Tsai, M. G.; Song, J. M.; Kempson, I. M.; Margaritondo, G. *Chem. Commun.* **2011**, *47*, 9152.
(34) Wang, C. L.; Hsao, B.; Lai, S.; Chen, W.; Chen, H. H.; Chen, Y. Y.; Chien, C. C.; Cai, X.; Kempson, I. M.; Hwu, Y.; Margaritondo, G. *Nanotechnology* **2011**, *22*, 065605.
(35) Wang, C. H.; Chien, C. C.; Yu, Y. L.; Liu, C. J.; Lee, C. H.; Chen, C. H.; Hwu, Y.; Yang, C. S.; Je, J. H.; Margaritondo, G. J. *Synchrotron Radiat.* **2007**, *14*, 477.
(36) Wang, C. H.; Liu, C. J.; Wang, C. L.; Hua, T. E.; Obliosca, J. M.; Lee, K. H.; Hwu, Y.; Yang, C. H.; Liu, R. H.; Lin, H. M.; Je, J. H.; Margaritondo, G. *J. Phys. D: Appl. Phys.* **2008**, *41*, 195301.
(37) Cai, X.; Wang, C. L.; Chen, H. H.; Chien, C. C.; Lai, S. F.; Chen, Y. Y.; Hua, T. E.; Kempson, I. M.; Hwu, Y.; Yang, C. S.; Margaritondo, G. *Nanotechnology* **2010**, *21*, 335604.
(38) Liu, C. J.; Wang, C. H.; Chien, C. C.; Yang, T. Y.; Chen, S. T.; Leng, W. H.; Lee, C. F.; Lee, K. H.; Hwu, Y.; Lee, Y. C.; Cheng, C. L.; Yang, C. S.; Chen, Y. J.; Je, J. H.; Margaritondo, G. *Nanotechnology* **2008**, *19*, 295104.
(39) Li, C.; Cai, W.; Li, Y.; Hu, J.; Liu, P. *J. Phys. Chem. B* **2006**, *110*, 1546.
(40) Ramnani, S. P.; Biswal, J.; Sabharwal, S. *Radiat. Phys. Chem.* **2007**, *76*, 1290.
(41) Radziuk, D. V.; Zhang, W.; Shchukin, D.; Möhwald, H. *Small* **2010**, *6*, 545.
(42) Millstone, J. E.; Hurst, S. J.; Métraux, G. S.; Cutler, J. I.; Mirkin, C. A. *Small* **2009**, *5*, 646.
(43) Germain, V.; Li, J.; Ingert, D.; Wang, Z. L.; Pileni, M. P. *J. Phys. Chem. B* **2003**, *107*, 8717.
(44) Lofton, C.; Sigmund, W. *Adv. Funct. Mater.* **2005**, *15*, 1197.
(45) Patakfalvi, R.; Virányi, Z.; Dékány, I. *Colloid Polym. Sci.* **2004**, *283*, 299.
(46) Dick, K.; Dhanasekaran, T.; Zhang, Z.; Meisel, D. *J. Am. Chem. Soc.* **2002**, *124*, 2312.
(47) Yoon, S. H.; Lee, J. H.; Lee, P. C.; Nam, J. D.; Jung, H. C.; Oh, Y. S.; Kim, T. S.; Lee, Y. K. *Macromol. Res.* **2009**, *17*, 568.
(48) Qin, Y.; Hu, M.; Li, H.; Zhang, Z.; Zou, Q. *Appl. Surf. Sci.* **2007**, *253*, 4021.
(49) Yeshchenko, O. A.; Dmitruk, I. M.; Alexeenko, A. A.; Kotko, A. V. *Nanotechnology* **2010**, *21*, 045203.
(50) Lu, H. M.; Li, P. Y.; Cao, Z. H.; Meng, X. K. *J. Phys. Chem. C* **2009**, *113*, 7598.
(51) Luo, W.; Su, K.; Li, K.; Liao, G.; Hu, N.; Jia, M. *J. Chem. Phys.* **2012**, *136*, 234704.
(52) Kim, N. H.; Kim, J. Y.; Ihn, K. J. *J. Nanosci. Nanotechnol.* **2007**, *7*, 3805.
(53) Van Eerdenbrugh, B.; Taylor, L. S. *Pharm. Res.* **2012**, *29*, 2754.